Computational Materials Science 144 (2018) 92–98

Contents lists available at ScienceDirect

Computational Materials Science

journal homepage: www.elsevier.com/locate/commatsci

Validation of inter-atomic potential for WS_2 and WSe_2 crystals through assessment of thermal transport properties

Arash Mobaraki [a], Ali Kandemir [b], Haluk Yapicioglu [c], Oğuz Gülseren [a], Cem Sevik [d,*]

[a] Department of Physics, Bilkent University, Ankara TR 06800, Turkey
[b] Department of Materials Science and Engineering, İzmir Institute of Technology, İzmir TR 35430, Turkey
[c] Department of Industrial Engineering, Faculty of Engineering, Anadolu University, Eskisehir TR 26555, Turkey
[d] Department of Mechanical Engineering, Faculty of Engineering, Anadolu University, Eskisehir TR 26555, Turkey

ARTICLE INFO

Article history:
Received 6 September 2017
Received in revised form 1 December 2017
Accepted 2 December 2017
Available online 16 December 2017

Keywords:
Interatomic potential
Transition metal dichalcogenides
Thermal conductivity
Spectral energy density

ABSTRACT

In recent years, transition metal dichalcogenides (TMDs) displaying astonishing properties are emerged as a new class of two-dimensional layered materials. The understanding and characterization of thermal transport in these materials are crucial for efficient engineering of 2D TMD materials for applications such as thermoelectric devices or overcoming general overheating issues. In this work, we obtain accurate Stillinger-Weber type empirical potential parameter sets for single-layer WS_2 and WSe_2 crystals by utilizing particle swarm optimization, a stochastic search algorithm. For both systems, our results are quite consistent with first-principles calculations in terms of bond distances, lattice parameters, elastic constants and vibrational properties. Using the generated potentials, we investigate the effect of temperature on phonon energies and phonon linewidth by employing spectral energy density analysis. We compare the calculated frequency shift with respect to temperature with corresponding experimental data, clearly demonstrating the accuracy of the generated inter-atomic potentials in this study. Also, we evaluate the lattice thermal conductivities of these materials by means of classical molecular dynamics simulations. The predicted thermal properties are in very good agreement with the ones calculated from first-principles.

1. Introduction

Single layer TMDs, MX_2 (M = Cr, Mo, and W and X = S, Se, Te) are a new class of two-dimensional materials which have been theoretically and experimentally proven to exhibit extraordinary properties such as intrinsic band gap, low thermal conductivity and chemical versatility [1] that make them ideal candidates for a vast range of applications where other well known 2D materials such as graphene and hexagonal boron nitride are inadequate. The fabrication and investigation of single and multi-layer MoS_2 [2,3], $MoSe_2$, $MoTe_2$ [4], WS_2 [5,6], and WSe_2 [7,8], as well as their heterostructures [9,10] for applications in practical technologies such as field-effect transistors [11,8,12] and logic circuits [13,14], energy storage [15], sensing [14], and catalysis [16] have already been pointed out. Given the importance of potential applications, an understanding of the thermal and vibrational properties of these materials has started to receive a lot of attention. Therefore, investigation of thermal and vibrational properties of these materials is essential and important.

The adaptation of common TMD compounds as potential thermoelectric materials [17–21] in energy harvesting, and cooling applications has been considered following the studies that report high power factor of MoS_2, and low lattice thermal conductivity of MoS_2 and WS_2. For instance, the Seebeck coefficient of bulk MoS_2 has been measured [22] as about 600 μV/K at around room temperature, which is larger than those of most good thermoelectric materials. Furthermore, remarkable Seebeck coefficient values as high as 10^5 μV/K has been observed in monolayer MoS_2 at low doping levels [23]. The highest predicted thermal conductivity among the aforementioned materials belongs to $MoSe_2$ reported as 33.6 $W\,m^{-1}\,K^{-1}$ which is much smaller than thermal conductivity of graphene. The lattice thermal conductivities of few layers MoS_2 [24–26], single layer WS_2 and double layers WS_2 [27] have been measured as 30.0–60.0 $W\,m^{-1}\,K^{-1}$, 32.0 $W\,m^{-1}\,K^{-1}$, and 53.0 $W\,m^{-1}\,K^{-1}$ respectively. Ultralow cross-planar thermal conductivity is measured for WSe_2 experimentally [28] and theoretically [29]. Using first principle calculations, Guo et al. [20] and Huang et al. [30] have determined the maximum dimensionless

* Corresponding author.
E-mail address: csevik@anadolu.edu.tr (C. Sevik).

https://doi.org/10.1016/j.commatsci.2017.12.005
0927-0256/

figure of merit (*ZT*), a measure for the performance of thermoelectric materials, of single layer MoS_2 as nearly 0.6. Additionally, using similar methods, a positive coefficient of thermal expansion at low temperatures has been reported for some of these materials [31,32] while for graphene it is reported to be negative [33]. Thermal and vibrational properties depend fundamentally on phonon properties. Aforementioned studies are based on density functional theory (DFT) which mostly used for ground state properties at zero temperature or on Boltzmann transport equation (BTE) which only considers the three phonon processes which may result in inaccurate prediction of phonon lifetimes and consequently thermal conductivity. From an experimental point of view, commonly used Raman techniques are very sensitive to sample quality and size and there are forbidden and mixed modes which might hinder the full investigation of phonon properties.

Molecular dynamics (MD) simulation is a powerful alternative which can overcome these difficulties but it requires a fairly accurate interatomic potentials. All anharmonic effects can be taken into account using spectral energy density (SED) which utilizes velocities obtained from MD simulations, thus considers all phonon processes [34]. Furthermore, MD may be used in order to investigate many effects which are not accessible easily in BTE and experimental studies, like defects, strain or deformations. The effects of temperature and phonon shifts in WS_2, WSe_2 and $MoSe_2$ are experimentally explored in various studies [35,36]. Furthermore, Anees et al. [37] utilized MD for studying the optical modes at Γ q-point in MoS_2. However, MD studies for W based materials are very limited, due to lack of accurate potentials except the recently published report [38] for WSe_2 which predicts the thermal conductivity notably less than the previous first principle calculations. Motivated by this, we developed a highly accurate Stillinger-Weber (SW) type interaction potential parameter sets (IPP) for WS_2 and WSe_2 monolayer structures by using the structural, mechanical and dynamical properties obtained from first-principles calculations. The resulting potentials give mechanical properties and phonon energies which are in very good agreement with DFT results. Then, we explored the effect of temperature on phonon energies and lifetimes using SED [34,39] and critically compared the results with previous experimental reports [35,36]. Finally, we systematically studied the thermal transport properties of these single layer materials by utilizing the Green-Kubo relations as derived from the fluctuation dissipation theorem.

2. Computational details

The desired value database used in SW type IPP optimization procedure is collected from first-principles pseudopotential plane-wave calculations based on density functional theory [40] by using the Vienna *ab initio* simulation package (VASP) [41–43]. Monolayers are placed in a supercell with a vacuum spacing of 20 Å along the perpendicular direction in order to avoid interaction between periodic images arised because of the periodic boundary conditions. The ions, so the core-valence interactions, are described by projector augmented wave type pseudopotentials (PAW) [44,45]. The exchange-correlation potential is treated within the generalized gradient approximation (GGA) following the Perdew-Burke-Ernzerhof (PBE) formulation. All computational parameters are determined after extensive test calculations ensuring good convergence of total energy and force calculations. Accordingly, a plane wave basis set is used with 500 eV kinetic energy cut-off. The Γ point centered $26 \times 26 \times 1$ Monkhorst-Pack *k*-point mesh is utilized for the Brillouin zone integrations. For the vibrational frequencies, first the force constants are calculated from density functional perturbation theory [46] as implemented in the VASP code, then the frequencies are obtained by using PHONOPY code [47], Here, $4 \times 4 \times 1$ conventional supercell structures (with $8 \times 8 \times 1$ Γ centered *k*-points grids) are considered for all crystals structures.

Following the first-principles calculations on structural, mechanical and dynamical properties of WS_2 and WSe_2, SW type IPP sets for both materials are attained by using Particle Swarm Optimization (PSO) algorithm as explicitly explained in our previous study [48]. The form of Stillinger-Weber (SW) inter-atomic potential parameters [49] incorporated in this study can be written as follows:

$$E = \sum_i \sum_{j>i} \phi_2(r_{ij}) + \sum_i \sum_{j\neq i} \sum_{k>j} \phi_3(r_{ij}, r_{ik}, \theta_{ijk}) \tag{1}$$

$$\phi_2(r_{ij}) = A_{ij}\left(\frac{B_{ij}}{r_{ij}^4} - 1\right) \exp\left[\frac{\rho_{ij}}{r_{ij} - r_{ij}^{max}}\right] \tag{2}$$

$$\phi_3(r_{ij}, r_{ik}, \theta_{ijk}) = K_{ijk} \exp\left[\frac{\rho_{ij}}{r_{ij} - r_{ij}^{max}} + \frac{\rho_{ik}}{r_{ik} - r_{ik}^{max}}\right] (\cos\theta_{ijk} - \cos\theta_{0,ijk})^2 \tag{3}$$

where ϕ_2 and ϕ_3 define the two-body (stretching) and three-body interactions (bond bending), respectively. In Eq. (1), the summation indices j and k are the indices of the neighbor atoms within the maximum distance of r^{max} from the atom i. The terms r_{ij} and r_{ik} are the separations between the pairs i,j and i,k, respectively. Remaining term θ_{ijk} is the angle between the radial vectors from centering atom i towards atoms j and k.

In Fig. 1, a few repeating units of the single layer WX_2 (X = S, Se) structures are schematically displayed from top and side. In order to describe this structure within the Stillinger-Weber inter-atomic potential outlined above, we need three stretching terms, namely for W-W, W-X and X-X, where X is the corresponding chalcogen atom. In contrary to the stretching, however for 3-body interactions, i.e. the angle bending, it is necessary to distinguish the chalcogen atoms because of the asymmetric chalcogen polyhedra around W. Therefore, the subscript u and d are introduced to represent the chalcogen atoms above and below the W layer, respectively, as seen on Fig. 1. Accordingly, three 3-body terms are defined as $X_{u,(d)}$-W-$X_{u,(d)}$, W-$X_{u,(d)}$-W and X_u-W-X_d. The first term describes the interactions for the configurations where the angle is between two chalcogens both above or below the W-plane and W atom at the center. The second term is for the configurations where the angle is in between two W's and a chalcogen (either above or below the W-plane) at the center. The third term is for the remaining configuration where the angle is between two chalcogens (one above and one below the W-plane) and W at the center. As shown in Fig. 1, these angles are labeled as θ_1, θ_2, and θ_3 respectively. The corresponding SW IPP sets are generated in appropriate formats for widely-used MD codes GULP [50] and LAMMPS [51,52] and provided as Supplementary Materials. The lack of the three-body cutoff parameter, r_{23} in LAMMPS SW potential implementation is fixed by modifying the *pair_sw.cpp* module of the code (version 1Feb14), which is provided as Supplementary Materials. For convenience, these two-body and three-body Stillinger-Weber parameters obtained by using the PSO are presented in Tables 1 and 2, respectively, in GULP format.

The phonon dispersion curves describing vibrational properties of solids can be obtained from MD simulations by two common approaches, either by calculating the eigenvalues of the dynamical matrix constructed from the result of MD simulation by using Green's functions [53,54], or from the phonon frequencies and lifetimes obtained from SED [34,39]. Although, anharmonic effects which might be especially important at finite temperature are taken into account in both approaches, one advantage of the SED

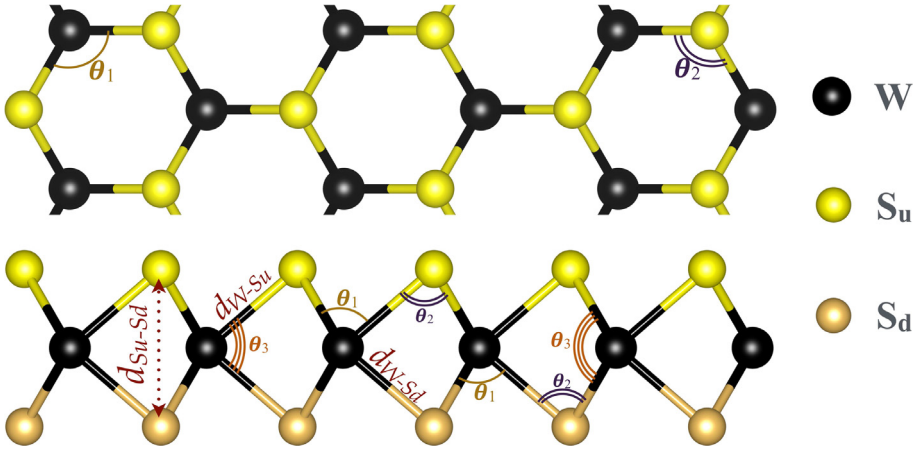

Fig. 1. Schematic representations (top and side views) of single layer WS_2 and WSe_2 structures.

Table 1
Two-body Stillinger-Weber parameters in GULP format.

	A	ρ	B	r_{min}	r_{max}
S-S	0.7701	0.1284	17.7001	0.00	3.80
W-S	8.8208	1.3972	16.1615	0.00	3.21
W-W	1.4797	0.7340	66.9509	0.00	4.35
Se-Se	1.6103	0.1000	20.0000	0.00	4.02
W-Se	10.0106	1.7403	19.2854	0.00	3.36
W-W	0.6120	0.1098	100.0000	0.00	4.53

Table 2
Three-body Stillinger-Weber parameters in GULP format.

	K	θ_0	ρ_{12}	ρ_{13}	r_{12}^{max}	r_{13}^{max}	r_{23}^{max}
W-$S_{u,d}$-$S_{u,d}$	19.5209	82.3451	1.054	1.054	3.21	3.21	3.80
$S_{u,d}$-W-W	19.5209	82.3451	1.054	1.054	3.21	3.21	4.35
W-S_u-S_d	0.1000	81.0412	1.054	1.054	3.21	3.21	3.80
W-$Se_{u,d}$-$Se_{u,d}$	20.0000	81.2948	1.3007	1.3007	3.36	3.36	4.02
$Se_{u,d}$-W-W	20.0000	81.2948	1.3007	1.3007	3.36	3.36	4.53
W-Se_u-Se_d	0.1000	82.4418	1.3007	1.3007	3.36	3.36	4.02

approach is that the SED provides more stable solutions near the Γ point [55]. There are several equivalent formulations for implementation of SED. One of the basic approach is based on the spatial Fourier transform of momentums [39]. Recently, a variant of this method that utilizes the *k*-space velocities was realized to investigate the temperature dependent phonon properties of graphene [55]. In this work, we follow the formulation of SED based on the atomic velocities in the crystal, simply inspired from the calculated phonon dispersion and lifetime of carbon nanotubes [34]. Moreover, it is also shown that this formulation and the one based on mode decomposition are equivalent [56]. In addition, in a comparative study of these two methods, equivalent results are reported for the h-BN system [57].

For a large simulation cell formed from N_c unit cells with n basis atoms in each unit cell, the SED is given as follows:

$$\Phi(k,\omega) = \frac{1}{4\pi\tau_0}\sum_{\alpha=1}^{3}\sum_{\beta=1}^{n}\frac{m_\beta}{N_c}\left|\sum_{=1}^{N_c}\int_0^{\tau_0} v_\alpha^{l,\beta} e^{ik.r_0 - i\omega t}dt\right|^2 \quad (4)$$

where τ_0 is the total simulation time, m_β is the mass of each basis atom, $v_\alpha^{l,\beta}$ is the velocity along the α direction of the basis atom β in unit cell l, and r_0 is the equilibrium position of the each atom. The SED exhibit sharp peaks at phonon frequencies ω_0 and each of these peaks can be described by a Lorentzian function of the following form:

$$\frac{A}{1+\left(\frac{\omega-\omega_0}{\gamma}\right)^2}. \quad (5)$$

where A is the intensity, the ω_0 is the phonon frequency, and γ is the broadening, i.e. the half width at half maximum. Therefore, the accurate position of the peak can be obtained from a Lorentzian fitting to each peak in SED, and then the phonon lifetime is simply given by $\frac{1}{2\gamma}$. All MD simulations in this work are carried out using LAMMPS. In all cases reported in this study, we constructed a 70 × 70 (14,700 atoms) triclinic computational cell. In MD simulations, equilibration is essential before the data analysis. The energy minimization is performed using conjugate gradient method. First, the systems are relaxed at desired pressure and temperature for 500 ps. Then, the data are collected in microcanonical ensemble for analysis. It is known that averaging over many simulations gives better results than a single long simulation [55,58]. Therefore, the results reported here are obtained by averaging over 8 simulations each lasted for about 500 ps (2^{20} time steps) using time step equal to 0.5 fs.

Eventually, phonon thermal transport properties of the materials are investigated by using the Green-Kubo relations which are

based on the fluctuation dissipation theorem [59,60]. The details of this approach were described previously [48]. The thermal conductivity, κ, values are calculated from a very good statistics based on the average of the results of seven distinct MD simulations carefully initialized, each have been started with different initial particle velocities. In these κ calculations, before the data collection, the systems were allowed to relax for 500 ps, and then let to evolve for a minimum of 5 ns with a time step of 0.5 fs in micro canonical ensemble for data collection. Previously, it was reported that this time duration is long enough to calculate the κ in graphene [61] and h-BN [62]. Given the fact that both graphene and h-BN have higher thermal conductivity, thus longer heat current autocorrelation tail than the studied TMDs, this simulation length is long enough for the studied systems. Another critical parameter is the cross-sectional area of the layered structure, $[(w \times \Delta)]$, where w is the width of the considered layered material, and Δ is set to the mean Van der Waals distance of the hexagonal bulk crystal, (0.612 nm for WS_2, and 0.648 nm WSe_2).

3. Results

As mentioned above, the lattice parameters (a_0), the distance between two nearest chalcogen atoms, each on the other side with respect to the W layer, one above and one below, ($d_{X_u X_d}$), elastic constants (C_{11} and C_{12}), Young's moduli (Y), and Poisson's ratio (ν) are included as parameters in the potential fitting procedure. Eventually, corresponding results obtained from both SW-IPP and DFT are compared for both single layer WS_2 and WSe_2, and they are in good agreement as seen from Table 3. In addition to these structural and mechanical properties, we also incorporate the vibrational properties in the SW-IPP training set for two purposes. First, is to describe the vibrational spectroscopic properties correctly, second is to accurately capture the correct lattice thermal transport behavior of the considered materials. At the first step, the phonon frequencies regarding the vibrational modes of these materials are calculated from first principles based density functional perturbation theory calculations.

In Fig. 2 (a) and (b), we compare the phonon dispersion along the high-symmetry directions of the Brilliuon zone for both materials as obtained from both DFT and SW-IPP. The dispersion diagram of both materials are very similar to each other except that WS_2 has higher mode frequencies compared to WSe_2. This is in line with the prediction of larger elastic constants and Young's moduli for WS_2 and can be mainly attributed to the mass difference between the S and Se. The SW-IPP results are in quite good agreement with those obtained from DFT calculations. In particular, the results clearly indicate the significant accuracy of the generated potential for the longitudinal, transverse, and out-of-plane acoustic branches (LA, TA and ZA), which plays significant role in thermal transport properties.

Equipped with the potential, we next investigated the effect of temperature on optical modes at the Γ point. In Fig. 3 the SEDs obtained from MD simulations are shown for WS_2 at T = 300 K. The line-shape of these results show a very good agreement with

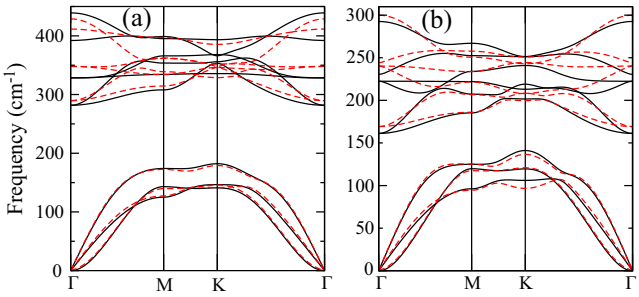

Fig. 2. (a) Phonon frequencies of (a) WS_2 and (b) WS_2 structures along high-symmetry directions of the Brillouin zone. Here, black solid lines and red dashed lines, SW represent the frequencies calculated from density functional perturbation theory (DFT) and generated potential parameters set (SW), respectively. (For interpretation of the references to colour in this figure legend, the reader is referred to the web version of this article.)

a Lorentzian function. As mentioned before, SED takes into account all anharmonic effects. In Fig. 4(a) and (b), the ratio of Γ point frequencies at different temperatures to those obtained at 300 K are shown for WS_2 and WSe_2. All optical modes at Γ point undergo a linear red-shift with increasing temperature. In Fig. 4(c) and (d), phonon linewidths for WS_2 and WSe_2 are shown. These results show that the line widths are increasing linearly with increasing temperature, so consequently the phonon lifetimes are decreasing with temperature. Note that the melting temperature of the bulk WS_2 and WSe_2 are around 1200 K and the Debye temperatures obtained from the maximum frequencies corresponding to the LA and TA modes are ~205 and ~150 K respectively. It is well known that BTE is valid only in the temperatures far from melting point were the high order terms are negligible. In the same vein, quantum effects are dominant at low temperatures below Debye temperature. Therefore, we restricted our discussion of temperature dependence from 200 K to 600 K especially for the phonon linewidths.

In Fig. 5, we display the phonon frequencies obtained from MD, shifted to match previously reported experimental values [35,36] in order to compare the trend in phonon frequency with increasing temperature. From Fig. 5, it is clear that our result are in perfect agreement with experimental data for WS_2. For WSe_2 there is a deviation from the experimental data, especially for the A_{1g} mode. However, the experimental data itself show a marked deviation from the expected linear trend. These results also indicate high accuracy of the SW-IPPs obtained in this work. Furthermore, this work includes the effect of temperature on experimentally forbidden modes as well.

Last, we report thermal conductivities at different temperatures in Fig. 6. As we described in Section 2, the classical description of atomic motion at equilibrium within fluctuation dissipation theory is used to calculate the in-plane lattice thermal conductivities of pristine WS_2 and WSe_2. The κ of WS_2 is observed to decrease from ~150 to ~100 W m^{-1} K^{-1} within the 200–500 K temperature range. In the case of WSe_2, κ decreases from ~50 to ~30 W m^{-1}

Table 3
The lattice parameter (a_0), the distance between two nearest chalcogen atoms one above and one below the W layer ($d_{X_u X_d}$), elastic constants (C_{11} and C_{12}), Young's modulus (Y), and Poisson's ratio (ν) of WS_2 and WSe_2 calculated with both DFT and the generated potential parameters set.

	a_0 (Å)	$d_{S,Se}$ (Å)	C_{11} (N/m)	C_{12} (N/m)	Y (N/m)	ν
WS_2						
DFT	3.18	1.57	146.5	31.8	139.6	0.22
SW	3.21	1.49	136.4	37.4	126.1	0.27
WSe_2						
DFT	3.32	1.50	120.4	23.1	116.0	0.19
SW	3.37	1.54	112.5	33.2	102.7	0.29

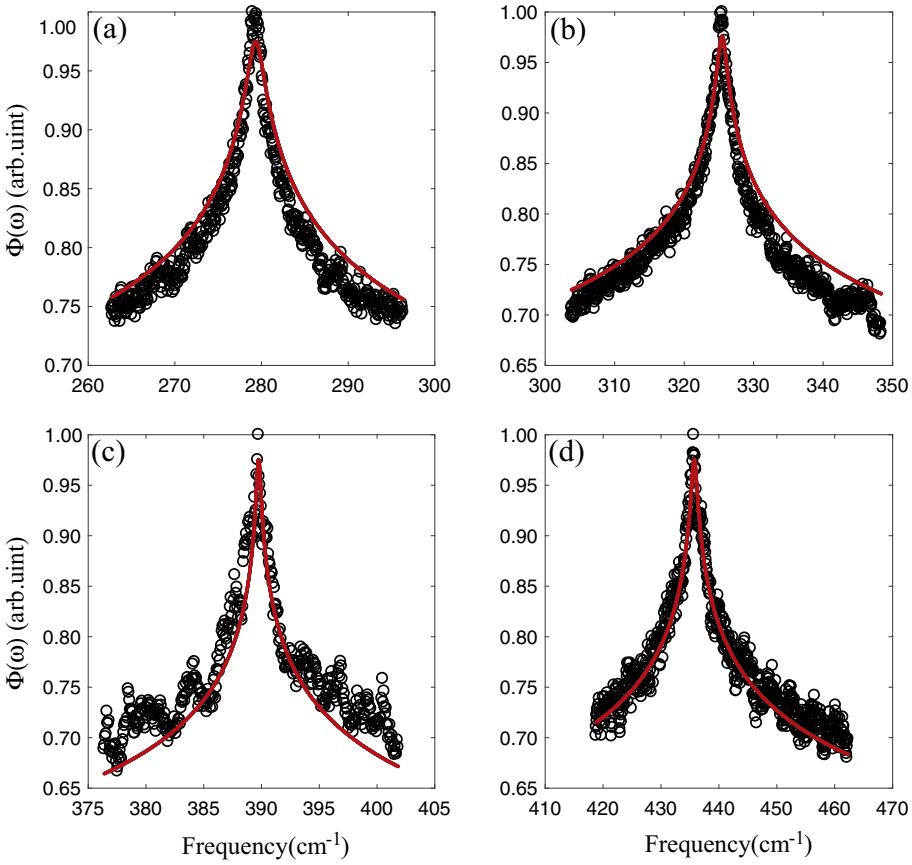

Fig. 3. Normalized SEDs (black circles) and Lorentzian fit (red lines) for WS_2 for (a) E_{1g}, (b) E^1_{2g}, (c) A_{1g} and (d)A_{2g} modes at T = 300 K. (For interpretation of the references to colour in this figure legend, the reader is referred to the web version of this article.)

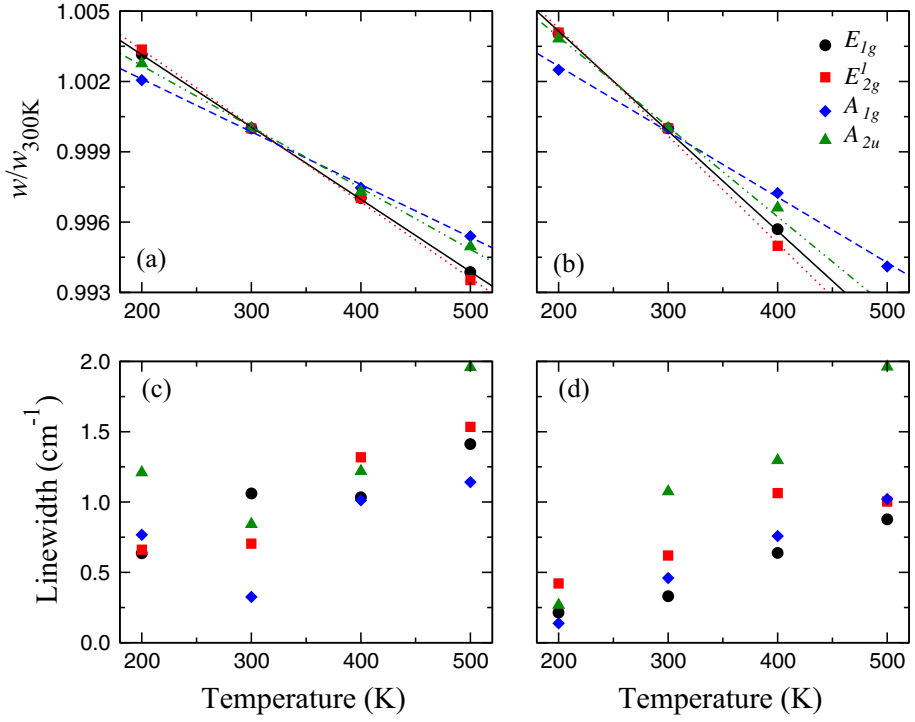

Fig. 4. Ratio of phonon frequencies to frequency at 300 K and linewidths at Γ as a function of temperature: for WS_2 (a) and (c), for WSe_2 (b) and (d).

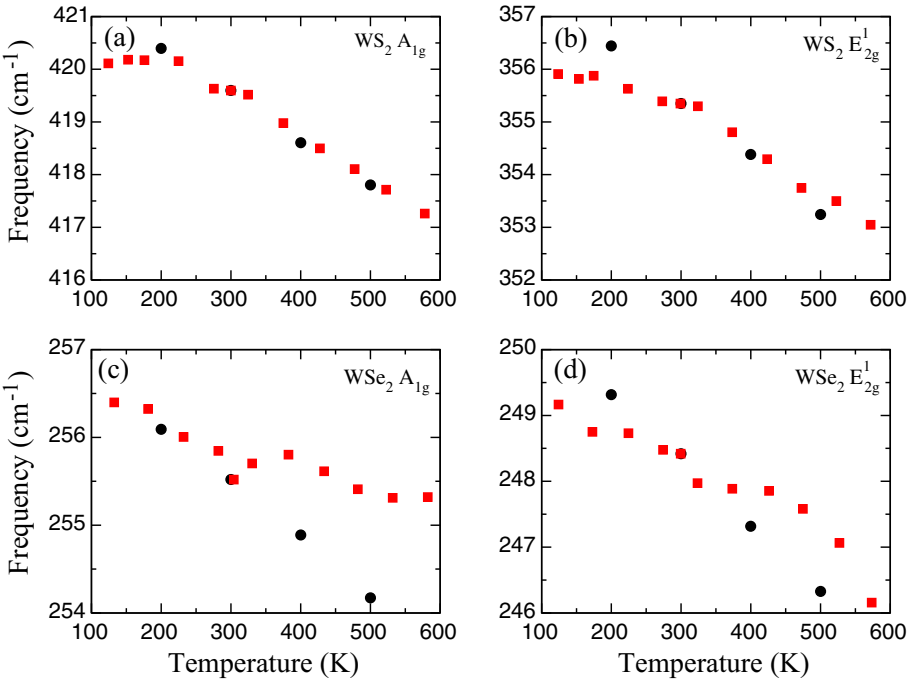

Fig. 5. Phonon frequencies at Γ as a function of temperature; both experimental data (red squares) and MD results (black circles) are shown. Experimental data taken from Refs. [35,36]. (For interpretation of the references to colour in this figure legend, the reader is referred to the web version of this article.)

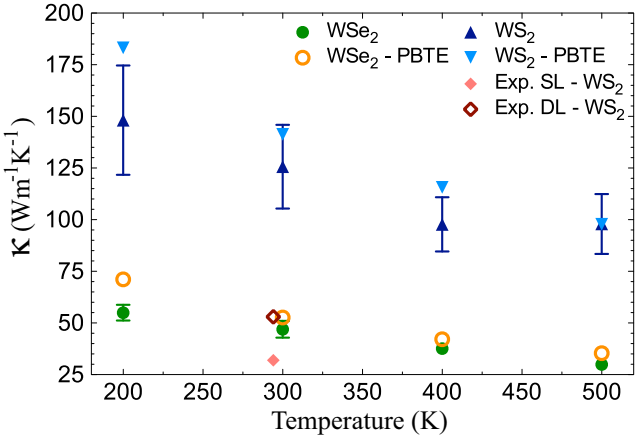

Fig. 6. Calculated thermal conductivity values of as a function of temperature. The theoretical (PBTE [63] results for single layer materials, and experimental measurements for single (Exp-SL [27]) and double (Exp-DL [27]) layers WS_2 structures are also presented.

K^{-1} within the same temperature range. We also present the values computed with Boltzmann transport calculations, in which phonon-phonon scattering rates are exactly obtained by using third order anharmonic interatomic force constants [63] in Fig. 6. As seen, our results agree with the reported first principles calculations very well throughout the considered temperature range.

4. Conclusion

Owing to their electronic and thermal properties, TMDs are proposed as a potential two-dimensional layered material to be used in next generation applications. In this respect, vibrational and thermal properties of WS_2 and WSe_2 are investigated by means of systematic MD simulations. In this work, Stillinger-Weber type empirical potential parameter sets for both materials are generated by using a stochastic search algorithm, namely particle swarm optimization. These empirical potentials are then validated by comparing several physical quantities also determined with DFT calculations. Then, by using this developed potential parameters temperature dependence of phonon linewidths and lifetimes on layered WS_2 and WSe_2 are investigated in detail. The observed frequency shifts with temperature agree with available experimental reports. The lattice thermal transport properties calculated by using generated parameter sets are also in very good agreement with existing reports from first-principle studies and experimental measurements. This further demonstrates the robustness and accuracy of the developed inter-atomic potential in this study.

Acknowledgment

This work was supported by Scientific and Technological Research Council of Turkey (TUBITAK-115F024) and Anadolu University (BAP-1407F335, -1705F335). Also, a part of this work was supported by the BAGEP Award of the Science Academy. Computational resources were provided by TUBITAK ULAKBIM, High Performance and Grid Computing Center (TRGrid e-Infrastructure), İstanbul Technical University, National Center for High Performance Computing (UHeM).

Appendix A. Supplementary material

Supplementary data associated with this article can be found, in the online version, at https://doi.org/10.1016/j.commatsci.2017.12.005.

References

[1] M. Chhowalla, H.S. Shin, G. Eda, L.-J. Li, K.P. Loh, H. Zhang, Nat. Chem. 5 (2013) 263.
[2] B. Radisavljevic, A. Radenovic, J. Brivio, V. Giacometti, A. Kis, Nat. Nano 6 (2011) 147.
[3] C. Lee, H. Yan, L.E. Brus, T.F. Heinz, J. Hone, S. Ryu, ACS Nano 4 (2010) 2695.

[4] J.N. Coleman, M. Lotya, A. O'Neill, S.D. Bergin, P.J. King, U. Khan, K. Young, A. Gaucher, S. De, R.J. Smith, I.V. Shvets, S.K. Arora, G. Stanton, H.-Y. Kim, K. Lee, G. T. Kim, G.S. Duesberg, T. Hallam, J.J. Boland, J.J. Wang, J.F. Donegan, J.C. Grunlan, G. Moriarty, A. Shmeliov, R.J. Nicholls, J.M. Perkins, E.M. Grieveson, K. Theuwissen, D.W. McComb, P.D. Nellist, V. Nicolosi, Science 331 (2011) 568.
[5] A.L. Elías, N. Perea-López, A. Castro-Beltrán, A. Berkdemir, R. Lv, S. Feng, A.D. Long, T. Hayashi, Y.A. Kim, M. Endo, H.R. Gutiérrez, N.R. Pradhan, L. Balicas, T.E. Mallouk, F. López-Urías, H. Terrones, M. Terrones, ACS Nano 7 (2013) 5235.
[6] H.R. Gutiérrez, N. Perea-López, A.L. Elías, A. Berkdemir, B. Wang, R. Lv, F. López-Urías, V.H. Crespi, H. Terrones, M. Terrones, Nano Lett. 13 (2013) 3447.
[7] J.-K. Huang, J. Pu, C.-L. Hsu, M.-H. Chiu, Z.-Y. Juang, Y.-H. Chang, W.-H. Chang, Y. Iwasa, T. Takenobu, L.-J. Li, ACS Nano 8 (2014) 923.
[8] W. Liu, J. Kang, D. Sarkar, Y. Khatami, D. Jena, K. Banerjee, Nano Lett. 13 (2013) 1983.
[9] S. Tongay, D.S. Narang, J. Kang, W. Fan, C. Ko, A.V. Luce, K.X. Wang, J. Suh, K.D. Patel, V.M. Pathak, J. Li, J. Wu, Appl. Phys. Lett. 104 (2014) 012101.
[10] J. Kang, J. Li, S.-S. Li, J.-B. Xia, L.-W. Wang, Nano Lett. 13 (2013) 5485.
[11] S. Larentis, B. Fallahazad, E. Tutuc, Appl. Phys. Lett. 101 (2012) 223104.
[12] A. Dankert, L. Langouche, M.V. Kamalakar, S.P. Dash, ACS Nano 8 (2014) 476.
[13] Q.H. Wang, K. Kalantar-Zadeh, A. Kis, J.N. Coleman, M.S. Strano, Nat. Nano 7 (2014) 699.
[14] D. Jariwala, V.K. Sangwan, L.J. Lauhon, T.J. Marks, M.C. Hersam, ACS Nano 8 (2014) 1102.
[15] H. Wang, H. Feng, J. Li, Small 10 (2014) 2165.
[16] M. Chhowalla, H.S. Shin, G. Eda, L.-J. Li, K.P. Loh, H. Zhang, Nat. Chem. 5 (2013) 263.
[17] C. Lee, J. Hong, M.-H. Whangbo, J.H. Shim, Chem. Mater. 25 (2013) 3745.
[18] W. Huang, X. Luo, C.K. Gan, S.Y. Quek, G. Liang, Phys. Chem. Chem. Phys. 16 (2014) 10866.
[19] W. Huang, H. Da, G. Liang, J. Appl. Phys. 113 (2013) 104304.
[20] H. Guo, T. Yang, P. Tao, Y. Wang, Z. Zhang, J. Appl. Phys. 113 (2013) 013709.
[21] D.D. Fan, H.J. Liu, L. Cheng, P.H. Jiang, J. Shi, X.F. Tang, Appl. Phys. Lett. 105 (2014) 133113.
[22] R. Mansfield, S.A. Salam, Proc. Phys. Soc. Sect. B 66 (1953) 377.
[23] M. Buscema, M. Barkelid, V. Zwiller, H.S.J. van der Zant, G.A. Steele, A. Castellanos-Gomez, Nano Lett. 13 (2013) 358.
[24] I. Jo, M.T. Pettes, E. Ou, W. Wu, L. Shi, Appl. Phys. Lett. 104 (2014) 201902.
[25] S. Sahoo, A.P.S. Gaur, M. Ahmadi, M.J.F. Guinel, R.S. Katiyar, J. Phys. Chem. C 117 (2013) 9042.
[26] R. Yan, J.R. Simpson, S. Bertolazzi, J. Brivio, M. Watson, X. Wu, A. Kis, T. Luo, A.R. Hight Walker, H.G. Xing, ACS Nano 8 (2014) 986.
[27] N. Peimyoo, J. Shang, W. Yang, Y. Wang, C. Cong, T. Yu, Nano Res. 8 (2015) 1210.
[28] C. Chiritescu, D.G. Cahill, N. Nguyen, D. Johnson, A. Bodapati, P. Keblinski, P. Zschack, Science 315 (2007) 351.
[29] W.-X. Zhou, K.-Q. Chen, Scient. Rep. 5, 15070 EP (2015), article.
[30] W. Huang, H. Da, G. Liang, J. Appl. Phys. 113 (2013) 104304.
[31] B. Peng, H. Zhang, H. Shao, Y. Xu, X. Zhang, H. Zhu, RSC Adv. 6 (2016) 5767.
[32] C. Sevik, Phys. Rev. B 89 (2014) 035422.
[33] B.D. Kong, S. Paul, M.B. Nardelli, K.W. Kim, Phys. Rev. B 80 (2009) 033406.
[34] J.A. Thomas, J.E. Turney, R.M. Iutzi, C.H. Amon, A.J.H. McGaughey, Phys. Rev. B 81 (2010) 081411.
[35] M. Thripuranthaka, D.J. Late, ACS Appl. Mater. Interfaces 6 (2014) 1158, pMID: 24364533.
[36] D.J. Late, S.N. Shirodkar, U.V. Waghmare, V.P. Dravid, C.N.R. Rao, ChemPhysChem 15 (2014) 1592.
[37] P. Anees, M.C. Valsakumar, B.K. Panigrahi, Appl. Phys. Lett. 108 (2016) 101902.
[38] P. Norouzzadeh, D.J. Singh, Nanotechnology 28 (2017) 075708.
[39] P.D. Ditlevsen, P. Stoltze, J.K. Norskov, Phys. Rev. B 44 (1991) 13002.
[40] D.A. McQuarrie, Electronic Structure, Cambridge University Press, Cambridge, England, 2004.
[41] G. Kresse, J. Hafner, Phys. Rev. B 47 (1993) 558.
[42] G. Kresse, J. Furthmüller, Phys. Rev. B 54 (1996) 11169.
[43] G. Kresse, J. Furthmüller, Comput. Mater. Sci. 6 (1996) 15.
[44] P.E. Blöchl, Phys. Rev. B 50 (1994) 17953.
[45] G. Kresse, D. Joubert, Phys. Rev. B 59 (1999) 1758.
[46] S. Baroni, S. de Gironcoli, A. Dal Corso, P. Giannozzi, Rev. Mod. Phys. 73 (2001) 515.
[47] A. Togo, F. Oba, I. Tanaka, Phys. Rev. B 78 (2008) 134106.
[48] A. Kandemir, H. Yapicioglu, A. Kinaci, T. çağın, C. Sevik, Nanotechnology 27 (2016) 055703.
[49] F.H. Stillinger, T.A. Weber, Phys. Rev. B 31 (1985) 5262.
[50] J.D. Gale, A.L. Rohl, Mol. Simul. 29 (2003) 291.
[51] S. Plimpton, J. Comput. Phys. 117 (1995) 1.
[52] "Lammps," (accessed May 25, 2015).
[53] C. Campañá, M.H. Müser, Phys. Rev. B 74 (2006) 075420.
[54] L.T. Kong, Comput. Phys. Commun. 182 (2011) 2201.
[55] E.N. Koukaras, G. Kalosakas, C. Galiotis, K. Papagelis, Scient. Rep. 5, 12923 EP (2015).
[56] T. Feng, B. Qiu, X. Ruan, J. Appl. Phys. 117 (2015) 195102, https://doi.org/10.1063/1.4921108.
[57] P. Anees, M.C. Valsakumar, B.K. Panigrahi, Phys. Chem. Chem. Phys. 18 (2016) 2672.
[58] Z.-Y. Ong, E. Pop, J. Shiomi, Phys. Rev. B 84 (2011) 165418.
[59] M.S. Green, J. Chem. Phys. 22 (1954) 398.
[60] R. Kubo, J. Phys. Soc. Japan 12 (1957) 570.
[61] J. Haskins, A. Kinaci, C. Sevik, H. Sevinçli, G. Cuniberti, T. Çağın, ACS Nano 5 (2011) 3779.
[62] C. Sevik, A. Kinaci, J.B. Haskins, T. Çağın, Phys. Rev. B 86 (2012) 075403.
[63] X. Gu, R. Yang, Appl. Phys. Lett. 105 (2014) 131903.